

# Particle-Hole Pair Coherence in Mott Insulator Quench Dynamics

K. W. Mahmud,<sup>1</sup> L. Jiang,<sup>1</sup> P. R. Johnson,<sup>2</sup> and E. Tiesinga<sup>1</sup>

<sup>1</sup>*Joint Quantum Institute, National Institute of Standards and Technology and University of Maryland, 100 Bureau Drive, Mail Stop 8423, Gaithersburg, Maryland 20899, USA*

<sup>2</sup>*Department of Physics, American University, Washington, DC 20016, USA*

We predict the existence of novel collapse and revival oscillations that are a distinctive signature of the short-range off-diagonal coherence associated with particle-hole pairs in Mott insulator states. Starting with an atomic Mott state in a one-dimensional optical lattice, suddenly raising the lattice depth freezes the particle-hole pairs in place and induces phase oscillations. The peak of the quasi-momentum distribution, revealed through time of flight interference, oscillates between a maximum occupation at zero quasi-momentum (the  $\Gamma$  point) and the edge of the Brillouin zone. We find that the population enhancements at the edge of the Brillouin zone is characteristic of coherent particle-hole pairs, and we show similar effects for fermions and Bose-Fermi mixtures in a lattice. Our results open a new avenue for probing strongly correlated many-body states with short-range phase coherence that goes beyond the familiar collapse and revivals previously observed in the long-range coherent superfluid regime.

PACS numbers: 03.75.-b, 67.85.-d, 72.20.-i

Ultracold atoms in optical lattices are a versatile tool for creating strongly correlated quantum many-body states [1, 2]. Prominent examples include atomic Mott insulator (MI) states of bosons and fermions [3–5]. Starting from a superfluid (SF) with long-range phase coherence, adiabatically increasing the ratio of atom-atom interaction  $U$  to tunneling strength  $J$  by increasing the optical lattice depth gives rise to a MI with short-range coherence [3]. An infinitely deep lattice with  $J = 0$  gives a *perfect* Mott insulator state as depicted in Fig. 1(a), denoted in Fock space notation as  $|11..11\rangle$  for unit occupancy. For finite tunneling but still in the MI regime, the many-body wavefunction includes correlated (paired) double and zero occupied sites on top of the perfect MI [see Fig. 1(b), (c)]. These particle-hole pairs, also known as doublons and holons and denoted as  $|201..1\rangle$ ,  $|210..1\rangle$ , etc., behave as quasi-particle excitations. Particle-hole pairs play an important role in Mott insulator physics [6–8], and have recently been observed by *in-situ* imaging in a one-dimensional (1D) chain of bosonic atoms [9].

Ultracold atoms in optical lattices are also a versatile tool for studying many-body quantum dynamics [10, 11]. A common technique involves quenching a system by suddenly changing its parameters [10, 12]. One approach, starting from larger  $U/J$  and quenching to a smaller  $U/J$ , has been used to study thermalization [13, 14], the Kibble-Zurek mechanism [15, 16], and light-cone spreading of correlations [17–19]. The opposite approach, starting in a SF regime with small  $U/J$  and quenching to large  $U/J$  gives the collapse-and-revival (CR) oscillations of matter-wave phase coherence observed in Refs. [20–22]. Matter-wave CR has found applications in the study of higher-body interactions [22, 23], fermion impurities [24], and coherent-state squeezing [22, 25]. To date, CR has been viewed as a characteristic behavior of quenched systems with long-range phase coherence such as superfluids.

In this Letter, we show that collapse-and-revival also occurs for quenched MI states, for both lattice bosons,

fermions, and mixtures. Surprisingly, detectable CR oscillations should occur despite the short-range coherence of the Mott state. For a 1D optical lattice, the quasi-momentum distribution oscillates between maximum occupations (revivals) at quasi-momentum  $\hbar k = 0$  and at the edge of the Brillouin zone. (Here  $\hbar = h/(2\pi)$  and  $h$  is Planck’s constant.) In fact, the normalized difference in the two populations, which is conventionally defined as the “visibility” of the condensate, becomes negative, in sharp contrast to the behavior of quenched superfluids. We also find that the visibility of the quenched MI state is a sinusoidal function of time, in contrast to the exponential functional form seen for quenched superfluids. This difference provides another approach for distinguishing between systems with short- and long-range coherence.

For a quenched MI, the condensate fraction oscillations also show novel kinks associated with oscillations between symmetric and antisymmetric natural orbitals

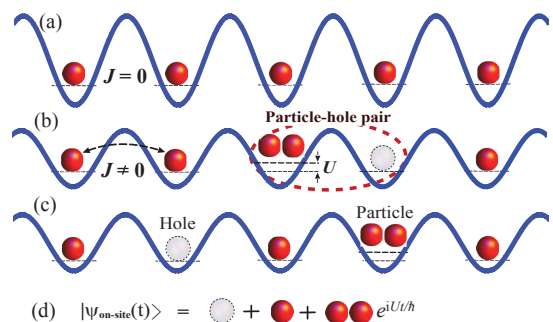


FIG. 1: (color online). A schematic of the Mott insulator state and quench. (a) A perfect Mott state with zero tunneling ( $J = 0$ ). For small tunneling  $J \neq 0$ , there exist nearest-neighbor and next-nearest-neighbor particle-hole pairs, as seen in (b) and (c), respectively. A sudden raise of the lattice depth freezes the atoms in place, and induces phase evolution of the on-site wavefunctions as schematically depicted in (d).

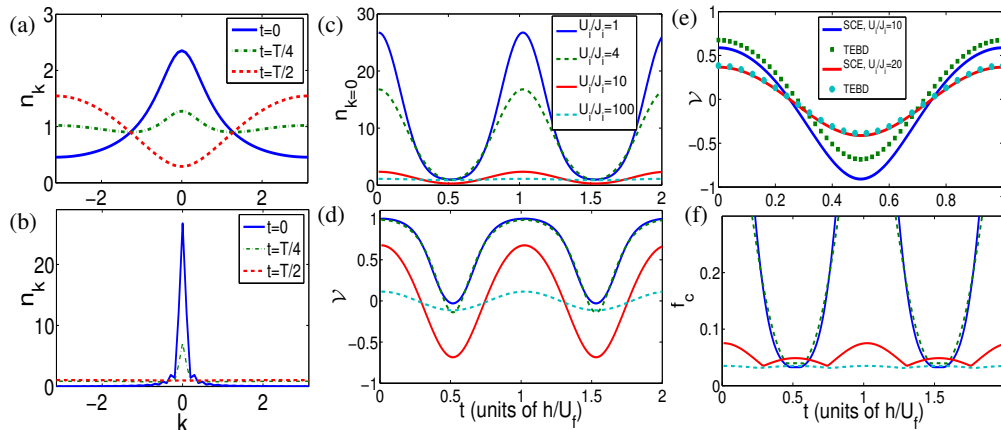


FIG. 2: (color online). Numerical simulations of Bosonic Mott-insulator coherence dynamics. (a) The quasi-momentum population  $n_k$  as a function of  $k$  for hold times  $t = 0, T/4$  and  $T/2$ , for a MI with occupation  $\bar{n} = 1$  and  $U_i/J_i = 10$ . During the collapse of the  $k = 0$  occupation, a revival occurs at the Brillouin zone edge at  $k = \pi$ . In contrast, (b) shows a SF quench for  $\bar{n} = 1.5$  and  $U_i/J_i = 1$ , where a collapse of the  $k = 0$  population is not accompanied by a revival at  $k = \pi$ . (c)  $n_{k=0}(t)$  as a function of hold time for four values of  $U_i/J_i$ , either in the SF or MI regimes, and  $\bar{n} = 1$ . (d) Visibility  $\mathcal{V}(t)$  dynamics for the same values of  $U_i/J_i$  as in (c) have a sinusoidal form and reach negative values (indicating  $n_{k=\pi} > n_{k=0}$ ) for MI states but not for SF. (e) A comparison between the strong-coupling expansion (SCE) theory and numerical i-TEBD results shows good agreement deep in the MI regime (e.g.,  $U_i/J_i = 20$ ) but not closer to the phase boundary (e.g.,  $U_i/J_i = 10$ ). (f) The condensate fraction  $f_c(t)$  dynamics, for the four  $U_i/J_i$  given in (c), shows novel kinks in the deep MI regime.

of the single-particle density matrix (SPDM). The distinctive behavior of MI CR oscillations are due to the presence of correlated particle-hole pairs, frozen in place when the lattice depth is suddenly increased, leading to phase dynamics as schematically illustrated in Fig. 1(d).

Unexpectedly, we find that fermions in a lattice at half-filling, and Bose-Fermi mixtures when the total occupation of bosons plus fermions is an integer, exhibit similar dynamics due to correlated particle-hole pairs. Finally, we show that this physics is robust under realistic dephasing mechanisms, and should be within experimental reach. Our results reveal universal coherence dynamics for quenched, strongly-correlated lattice systems with short-range phase coherence.

*Lattice bosons.*— Ultracold bosons in an optical lattice can be described by the Bose-Hubbard Hamiltonian

$$H_i^B = -J_i \sum_{\langle jj' \rangle} (b_j^\dagger b_{j'} + \text{h.c.}) + \frac{U_i}{2} \sum_j n_j (n_j - 1), \quad (1)$$

where  $j, j'$  are indices to lattice sites, only nearest-neighbor tunneling is assumed, and  $n_j = b_j^\dagger b_j$ . The subscript  $i$  denotes parameter values before the quench. The total number of particles is  $N = \sum_j \langle b_j^\dagger b_j \rangle$ , and  $\bar{n} = N/L$  is the mean occupation per site where  $L$  is the number of sites. For non-integer occupation per site, the ground state is superfluid. At integer occupation, the system exhibits a quantum phase transition, going from a SF to MI state above a critical value of  $\eta_c = U/J$ . At unit occupation,  $\eta_c \approx 3.37$  in 1D [26, 27].

The system is quenched by suddenly increasing the depth of the optical lattice such that tunneling is suppressed ( $J_f \rightarrow 0$ ) [20]. The Hamiltonian governing the post-quench dynamics is  $H_f = (U_f/2) \sum_j n_j (n_j - 1)$ ,

where  $U_f$  is the final interaction strength. After a hold-time  $t$ , the lattice is turned off and the atoms are allowed to freely expand. Imaging the atoms after the time-of-flight expansion, the atomic spatial density corresponds to the quasi-momentum distribution  $n_k(t) = (1/L) \sum_{j,j'} e^{ik(j-j')} \rho_{jj'}(t)$  at the moment of release, where  $\rho_{jj'}(t) = \langle b_j^\dagger b_{j'} \rangle$  is the SPDM and  $k$  is the lattice wavevector. In a 1D lattice with a period of unit length, the edge of the Brillouin zone is at wavevector  $k = \pi$ . In addition, we examine the visibility  $\mathcal{V}(t) = [n_{k=0}(t) - n_{k=\pi}(t)] / [n_{k=0}(t) + n_{k=\pi}(t)]$  [6], and the condensate fraction  $f_c(t) = \lambda_c(t)/N$ , where  $\lambda_c(t)$  is the largest eigenvalue of the SPDM [28, 29].

In previous CR studies the initial state is a superfluid. Here, our initial state is a one-dimensional MI with integer  $\bar{n}$  and  $U_i/J_i > \eta_c$ . Due to the presence of particle-hole pairs, this state, after the quench, is not an eigenstate of  $H_f$ , and undergoes nonequilibrium evolution until the moment of release from the lattice. Much of the MI quench dynamics can be understood from an analysis of correlations in the initial state. It is convenient to define the off-diagonal coherence  $\zeta_d(t) = \langle b_j^\dagger b_{j+d} \rangle$ , which is independent of  $j$  as the SPDM  $\rho_{jj'}$  only depends on  $|j - j'|$  for a homogeneous system with periodic boundary conditions. It follows that  $n_{k=0}(t) = \bar{n} + 2 \sum_{d>0} (1 - d/L) \zeta_d(t)$  and, similarly,  $n_{k=\pi}(t) = \bar{n} + 2 \sum_{d>0} (-1)^d (1 - d/L) \zeta_d(t)$ .

We are able to obtain explicit analytic approximations for the evolution of the off-diagonal coherence and quasimomentum populations for bosons in a 1D lattice using the strong-coupling expansion [30] up to second-order in the tunneling Hamiltonian. The full derivation is given in the Supplementary material. Briefly, to zeroth-order the ground-state wavefunction is the Mott state  $|0\rangle = |\bar{n}, \bar{n}, \dots, \bar{n}\rangle$  with  $\bar{n}$  atoms in each of the  $L$

sites. Corrections are due to states containing a “hole”,  $\bar{n} - 1$  atoms in one of the sites, and a “particle”,  $\bar{n} + 1$  atoms in another. We can express these particle-hole pair states as  $|e_d\rangle \propto \sum_{j=1}^L (b_j^\dagger b_{j+d} + b_{j+d}^\dagger b_j)|0\rangle$ , where  $d > 0$  is the lattice distance between particle and hole. The improved ground state becomes  $|g\rangle = |0\rangle + \sum_{d>0} \epsilon_d |e_d\rangle$  with  $\epsilon_d \propto (J_i/U_i)^d \ll 1$ , from which it follows that initially  $\zeta_d(t=0) \propto (J_i/U_i)^d$ . This corresponds to an exponential decay of the off-diagonal coherence with distance  $d$  (see also Ref. [31]).

Deep in the MI regime the time evolution of the  $k=0$  and  $k=\pi$  populations are therefore, to good approximation,  $n_{k=0}(t) \approx 1 + 2(1 - 1/L)\zeta_1(t)$  and  $n_{k=\pi}(t) \approx 1 - 2(1 - 1/L)\zeta_1(t)$ , respectively. Consequently, when  $\zeta_1(t)$  is positive (negative) the population  $n_{k=0}(t)$  is larger (smaller) than  $n_{k=\pi}(t)$ . In fact, it is shown in the Supplementary material that  $\zeta_1(t) \propto (J_i/U_i) \cos(U_f t/\hbar)$  with period  $T = h/U_f$ . Hence,  $n_{k=\pi}(t)$  is larger than  $n_{k=0}(t)$  for  $T/2 < t < 3T/2$ . This implies that  $\mathcal{V}(t) \propto n_{k=0}(t) - n_{k=\pi}(t) < 0$  for these hold times.

In contrast, for a SF with  $U_i/J_i < \eta_c$  (and non-integer  $\bar{n}$ ), the mean-field ground-state wavefunction is site separable, i.e., of the form  $\prod_j |S_j\rangle$ , with  $|S_j\rangle = \sum_n c_n^{(j)} |n\rangle$ . Consequently, the SPMD is also separable with  $\zeta_d = \langle b_j^\dagger \rangle \langle b_{j+d} \rangle$ . For a homogeneous lattice  $\zeta_d = |\langle b \rangle|^2$  is independent of  $d$  and there is no decay of correlation with particle-hole distance  $d$ . As all  $\zeta_d$  are positive we find  $n_{k=0}(t) \geq n_{k=\pi}(t)$  for all  $t$ . This implies that  $\mathcal{V}(t) > 0$ .

In the Supplementary material we also derive the quasi-momentum and visibility in the MI regime and the thermodynamic limit. They are given by

$$n_k(t) \approx \bar{n} + 4\bar{n}(\bar{n} + 1) \frac{J_i}{U_i} \cos\left(\frac{U_f t}{\hbar}\right) \cos(k) \quad (2)$$

$$+ 2\bar{n}(\bar{n} + 1)(2\bar{n} + 1) \frac{J_i^2}{U_i^2} \left[ 1 + 2 \cos\left(\frac{U_f t}{\hbar}\right) \right] \cos(2k),$$

and

$$\mathcal{V}(t) \approx 4(\bar{n} + 1) \frac{J_i}{U_i} \cos(U_f t/\hbar). \quad (3)$$

In contrast, in the superfluid regime with a homogeneous pre-quench state that is separable,  $n_{k=0}(t) = (L - 1)v(t) + \bar{n}$  and  $\mathcal{V}(t) = v(t)/(v(t) + 2[\bar{n} - v(t)]/L)$ , where  $v(t) = |\langle b(t) \rangle|^2$ . For a coherent state  $|\beta\rangle$  at each lattice site

$$v(t) = |\langle b(t) \rangle|^2 = \bar{n} e^{2\bar{n}[\cos(U_f t/\hbar) - 1]}, \quad (4)$$

where  $\bar{n} = |\beta|^2$  and  $b_j(t) = e^{iH_f t/\hbar} b_j e^{-iH_f t/\hbar} = e^{-iU_f n_j t/\hbar} b_j$ . For both the MI and SF quench the time evolution is periodic with period  $T = h/U_f$ . The oscillations, however, are sinusoidal for the MI quench and “exponential” for the SF quench.

We next perform numerical i-TEBD simulations [32] to extend our analysis to all values of  $U_i/J_i$  and validate the SCE analysis in the MI regime. We calculate the SPDM for  $L = 32$  and use periodic boundary conditions.

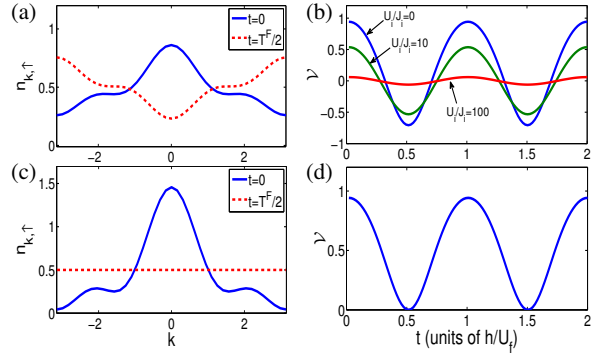


FIG. 3: (color online). Lattice fermions. (a)  $n_{k,\uparrow}$  as a function of  $k$  at times  $t = 0$  and  $T^F/2$  for a half-filled state. (b) The visibility dynamics of the spin-up state shows sinusoidal oscillations for several  $U_i/J_i$ . Panels (c) and (d) show  $n_{k,\uparrow}$  versus  $k$  and spin-up visibility versus time, respectively, of a non-half-filled metallic state, with superfluid like CR.

Figure 2(a) shows the quasi-momentum  $n_k(t)$  for a Mott state with  $U_i/J_i = 10$  at hold times  $t = 0, T/4$ , and  $T/2$ . At  $t = 0$  the momentum distribution is peaked around  $k = 0$ , while at  $t = T/2$  it is peaked around  $k = \pi$ , corresponding to a “revival” at the edge of the Brillouin zone and to a new kind of nonequilibrium state. This  $n_{k=\pi}(t)$  revival is a distinctive signature of the presence of nearest-neighbor particle-hole pairs in the MI state.

To highlight the difference between MI and superfluid quenches, Fig. 2(b) shows the  $n_k(t)$  dynamics for a superfluid with  $U_i/J_i = 1$  and  $\bar{n} = 1.5$ . Here, at  $t = 0$  the quasimomentum distribution is again peaked around  $k = 0$ , but is much narrower than the MI case due to the long-range coherence of the SF. During the collapse at  $t = T/2$ , the atoms are equally spread over all quasi-momenta with no enhancement or revival of the  $k = \pi$  population. Note that  $n_{k=\pi}(t)$  revivals have also been predicted for supersolid quenches in a system with (long-range) nearest-neighbor interactions [33]. Those revivals, however, are associated with long-range coherences and not particle-hole pairs.

Figure 2(c) and (d) show the time evolution of  $n_{k=0}(t)$  and  $\mathcal{V}(t)$  for different values of  $U_i/J_i$  and  $\bar{n} = 1$ , one in the SF regime and three in the MI regime. For  $U_i/J_i = 1$ , the time trace exhibits superfluid CR oscillations consistent with Eq. 4 and the visibility is positive. Based on our numerical results, we conjecture that for  $U_i/J_i > \eta_c$  there will always exist time intervals where the visibility is negative. We show an example for  $U_i/J_i = 4$  in Fig. 2(d). For larger  $U_i/J_i$  the oscillations in  $n_{k=0}(t)$  and  $\mathcal{V}(t)$  become more sinusoidal, consistent with Eqs. 2 and 3. Examples are given for  $U_i/J_i = 10$  and 100.

In Fig. 2(e) we compare analytic predictions for  $\mathcal{V}(t)$  in Eq. 3 with our numerical simulations. The analytic approximation gives excellent agreement for  $U_i/J_i \gtrsim 20$ . The regime of validity for the analytic theory can be extended to smaller  $U_i/J_i$  by performing higher-order calculations and keeping high occupancy terms, e.g., terms such as  $[\dots030\dots]$  and  $[\dots2020\dots]$  for unit occupancy ( $\bar{n} = 1$ ).

Figure 2(f) shows the condensate fraction  $f_c(t) =$

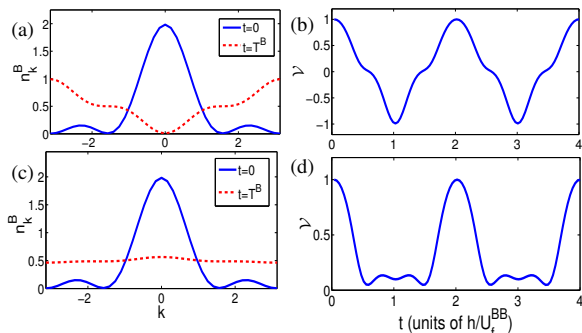


FIG. 4: (color online). Lattice Bose-Fermi mixtures. (a)  $n_k^B$  as a function of  $k$  at times  $t = 0$  and  $T^B/2$ , with  $T^B = h/U_f^{BB}$  and  $U_f^{BF}/U_f^{BB} = 0.5$ , and a combined unit occupation of bosons and fermions. A maximum in the  $k = \pi$  occupation occurs when the  $k = 0$  occupation is near zero (collapses). (b) The bosonic visibility shows MI-like sinusoidal features. In contrast, a state with non-integer combined occupation gives SF-like CR dynamics in  $n_k^B$  (c) and bosonic visibility (d).

$\lambda_c(t)/N$  as a function of time. For  $U_i/J_i$  in the MI regime  $f_c(t)$  has kinks at times  $t = T/4$  and  $3T/4$ , which occur when the eigenfunction or natural orbital of the SPDM associated with the largest eigenvalue changes between a symmetric state  $(1, 1, \dots, 1)$  and an anti-symmetric state  $(1, -1, \dots, 1, -1)$ . This behavior is consistent with our SCE calculations, which give

$$\lambda_c(t) = \bar{n} + 4\bar{n}(\bar{n} + 1) \frac{J_i}{U_i} |\cos(U_f t/\hbar)| + 2\bar{n}(\bar{n} + 1)(2\bar{n} + 1) \frac{J_i^2}{U_i^2} [1 + 2\cos(U_f t/\hbar)], \quad (5)$$

and where the second term leads to the kinks. Within the SCE approximation the kinks occur when the nearest neighbor coherence  $\zeta_{d=1}$  goes to zero. For  $U_i/J_i = 1$  in the SF regime the fraction performs smooth oscillations reaching one. (The full range is not shown in the graph.) The numerical result is consistent with  $f_c(t) = v(t)/\bar{n} + (\bar{n} - v(t))/N$ , based on the mean-field approximation [29].

*Lattice fermions.*— Fermions in an optical lattice are described by the Fermi-Hubbard Hamiltonian

$$H_i^F = -J_i^F \sum_{\langle jj' \rangle \sigma} (f_{j\sigma}^\dagger f_{j'\sigma} + \text{h.c.}) + U_i^F \sum_j n_{j\uparrow} n_{j\downarrow}, \quad (6)$$

where  $\sigma = \uparrow, \downarrow$  denotes two spin states and  $n_{j\sigma} = f_{j\sigma}^\dagger f_{j\sigma}$ . Its phase diagram contains metallic, Mott insulator and anti-ferromagnetic phases [34]. After the quench the Hamiltonian becomes  $H_f^F = U_f^F \sum_j n_{j\uparrow} n_{j\downarrow}$ . Figure 3 illustrates the quench dynamics, computed using a four site lattice and exact diagonalization. We first consider the half-filled case with  $\langle n_{j\uparrow} \rangle = \langle n_{j\downarrow} \rangle = 1/2$ . Figure 3(a) shows the momentum distribution  $n_{k,\uparrow}$  at times  $t = 0$  and  $T^F/2$ , where  $T^F = h/U_f^F$ . At  $t = 0$  the momentum distribution is peaked around  $k = 0$ , while at  $t = T^F/2$  the peak occurs at the edge of the Brillouin zone, an

effect similar to the bosonic MI case. The  $k = \pi$  revivals are again due to correlated doublons and holons in the initial state. Visibility oscillations of the spin-up state, shown in Fig. 3(b), reach negative values for any  $U_i/J_i$  and become more sinusoidal for larger values of  $U_i/J_i$ . In contrast, Figs. 3(c) and (d) show that a metallic state with  $\langle n_{j\uparrow} \rangle = 1/4$  and  $\langle n_{j\downarrow} \rangle = 1/2$  exhibits the familiar superfluid-type CR, where all quasi-momenta are uniformly occupied during collapse at  $t = T^F/2$ .

*Lattice Bose-Fermi mixtures.*— For Bose-Fermi mixtures in a lattice, the post-quench Hamiltonian is

$$H_f^{BF} = \frac{U_f^{BB}}{2} \sum_j n_j^B (n_j^B - 1) + U_f^{BF} \sum_j n_j^B n_j^F, \quad (7)$$

where  $U_f^{BB}$  and  $U_f^{BF}$  are Bose-Bose and Bose-Fermi interaction strengths, respectively, and assuming fermions in a single spin state. For the pre-quench Hamiltonian, the usual hopping terms are also present [35]. Bose-Fermi mixtures give rise to a plethora of phases and phenomena [35, 36], depending on the relative interaction strengths and fermion filling. CR of a Bose-Fermi mixture has been observed in Ref. [24]. When the total occupation per site of fermions plus bosons is one, the ground state phase diagram has a MI state [37]. The quench dynamics, computed with a four site lattice, is shown in Figs. 4(a) and (b). Here again we see  $k = \pi$  revivals of the bosonic momentum distribution  $n_k$  and the sinusoidal behavior of the bosonic visibility, with modifications due to the Bose-Fermi interaction. In contrast, for non-unit occupation, the dynamics gives the SF-like CR shown in Figs. 4(c) and (d).

*Experimental prospects and conclusions.*— Our analysis in Fig. 2 shows that the predicted visibility of the  $k = \pi$  revival should be of the same order of magnitude as the  $k = 0$  peak observed for an equilibrium MI [6], and hence a detection of the dynamics should be possible. These effects are also robust under several dephasing mechanisms. First, Fig. 5(a) shows that for small post-quench tunneling  $J_f$  the characteristic negative  $\mathcal{V}$  survives, but is destroyed for larger  $J_f/U_f$ . Second, we find that effective multi-body interactions [22, 38, 39] do not significantly influence the dynamics deep in the  $\bar{n} = 1$  MI regime (e.g.,

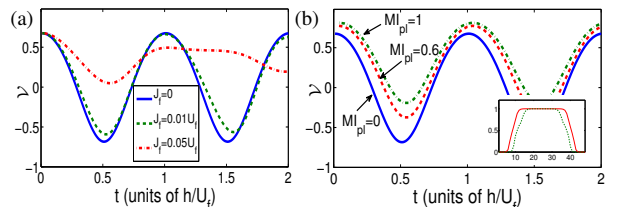


FIG. 5: (color online). Effects of residual tunneling and initial harmonic confinement on bosonic MI dynamics. (a) Visibility dynamics for three values of  $J_f$ . Other parameters as in Fig. 2(a). (b) Visibility dynamics for an initially trapped system for  $W_{pl} = 0, 0.6$ , and  $1$ , where  $W_{pl}$  is the ratio of the width of SF regions to the Mott plateau. Inset shows the initial density profile as a function of lattice site.

$U_i/J_i > 10$ ). Third, by adding  $V_{T,i} \sum_j (j - L/2)^2 n_j$  in Eq. 1, harmonically trapped systems give a MI core with SF regions at the two edges. Assuming  $V_{T,f} = 0$  after the quench, Fig. 5(b) shows that the SF regions modify  $\mathcal{V}(t)$ , but do not completely wash out the distinctive MI signature for a sufficiently large Mott plateau. Dephasing due to post-quench harmonic trapping  $V_{T,f} \neq 0$  for SF revivals has been quantified in Refs. [29, 40].

In conclusion, we have shown that bosons and fermions

in 1D periodic potentials with short-range coherence will manifest a new type of collapse-and-revival oscillation due to particle-hole pair correlations. We expect qualitatively similar effects in 2D and 3D. Our results open up the possibility that the underlying correlations of a wide class of strongly correlated matter can now be revealed through coherence dynamics.

*Acknowledgments.*— We acknowledge support from the US Army Research Office under Contract No. 60661PH.

- 
- [1] E. Duchon, Y. L. Loh, and N. Trivedi, e-print arXiv:1311.0543 (2013).
- [2] I. Bloch, J. Dalibard, and W. Zwerger, *Rev. Mod. Phys.* **80**, 885-964 (2008).
- [3] M. Greiner, O. Mandel, T. W. Hänsch and I. Bloch, *Nature* **415**, 39 (2002).
- [4] R. Jordens, N. Strohmaier, K. Gnter, H. Moritz, and T. Esslinger, *Nature* **455**, 7210 (2008).
- [5] U. Schneider, L. Hackermuller, S. Will, Th. Best, I. Bloch, T. A. Costi, R. W. Helmes, D. Rasch, and A. Rosch, *Science* **322**, 5907 (2008).
- [6] F. Gerbier, A. Widera, S. Foelling, O. Mandel, T. Gericke, and I. Bloch, *Phys. Rev. Lett.* **95**, 050404 (2005); *Phys. Rev. A* **72**, 053606 (2005).
- [7] W. S. Bakr, J. I. Gillen, A. Peng, S. Foelling, and M. Greiner, *Nature* **462**, 74 (2009).
- [8] W. S. Bakr, A. Peng, M. E. Tai, R. Ma, J. Simon, J. I. Gillen, S. Foelling, L. Pollet, and M. Greiner, *Science* **329**, 547 (2010).
- [9] M. Endres, M. Cheneau, T. Fukuhara, C. Weitenberg, P. Schauss, C. Gross, L. Mazza, M.C. Banuls, L. Pollet, I. Bloch, and S. Kuhr, *Science* **334**, 200 (2011).
- [10] M. P. Kennett, *ISRN Condensed Matter Physics*, **2013**, 393616 (2013).
- [11] A. Polkovnikov, K. Sengupta, A. Silva, and M. Vengalattore, *Rev. Mod. Phys.* **83**, 863 (2011); J. Dziarmaga, *Adv. Phys.* **59**, 1063 (2010).
- [12] C. Kollath, A. M. Laeuchli, and E. Altman, *Phys. Rev. Lett* **98**, 180601 (2007).
- [13] E. Altman and A. Auerbach, *Phys. Rev. Lett.* **89**, 250404 (2002).
- [14] M. Rigol, V. Dunjko, and M. Olshanii, *Nature* **452**, 854 (2008).
- [15] W. H. Zurek, U. Dorner and P. Zoller, *Phys. Rev. Lett.* **95**, 105701 (2005).
- [16] D. Chen, M. White, C. Borries and B. DeMarco, *Phys. Rev. Lett.* **106**, 235304 (2011).
- [17] M. Cheneau, P. Barmettler, D. Poletti, M. Endres, P. Schauss, T. Fukuhara, C. Gross, I. Bloch, C. Kollath, and S. Kuhr *et al.*, *Nature* **481**, 484 (2012).
- [18] P. Barmettler, D. Poletti, M. Cheneau, and C. Kollath, *Phys. Rev. A* **85**, 053625 (2012).
- [19] S. S. Natu and E. J. Mueller, *Phys. Rev. A* **87**, 063616 (2013).
- [20] M. Greiner, O. Mandel, T. W. Hänsch and I. Bloch, *Nature* **415**, 51 (2002).
- [21] J. Sebby-Strabley, B. L. Brown, M. Anderlini, P. J. Lee, W. D. Phillips, J. V. Porto, and P. R. Johnson, *Phys. Rev. Lett.* **98**, 200405 (2007).
- [22] S. Will, T. Best, U. Schneider, L. Hackermüller, D.-S. Lühmann, and I. Bloch, *Nature* **465**, 197 (2010).
- [23] K. W. Mahmud and E. Tiesinga, *Phys. Rev. A* **88**, 023602 (2013).
- [24] S. Will, T. Best, S. Braun, U. Schneider, and I. Bloch, *Phys. Rev. Lett.* **106**, 115305 (2011).
- [25] E. Tiesinga and P. R. Johnson, *Phys. Rev. A* **83**, 063609 (2011).
- [26] R. T. Scalettar, G. G. Batrouni, and G. T. Zimanyi, *Phys. Rev. Lett.* **66**, 3144 (1991).
- [27] J. Zakrzewski and D. Delande, *AIP Conf. Proc.* **1076**, 292 (2008).
- [28] O. Penrose and L. Onsager, *Phys. Rev.* **104**, 576 (1956).
- [29] M. Buchhold, U. Bissbort, S. Will, and W. Hofstetter, *Phys. Rev. A* **84**, 023631 (2011).
- [30] J. K. Freericks and H. Monien, *Phys. Rev. B* **53**, 2691 (1996).
- [31] M. A. Cazalilla, R. Citro, T. Giamarchi, E. Orignac, and M. Rigol, *Rev. Mod. Phys.* **83**, 1405-1466 (2011).
- [32] G. Vidal, *Phys. Rev. Lett.* **98**, 070201 (2007); **93**, 040502 (2004).
- [33] U. R. Fischer and B. Xiong, *Europhys. Lett.* **99**, 66003 (2012).
- [34] P. A. Lee and X.-G. Wen, *Rev. Mod. Phys.* **78**, 17 (2006).
- [35] A. Albus, F. Illuminati, and J. Eisert, *Phys. Rev. A* **68**, 023606 (2003).
- [36] P. Anders, P. Werner, M. Troyer, M. Sigrist, and L. Pollet, *Phys. Rev. Lett.* **109**, 206401 (2012).
- [37] E. Altman, E. Demler, and A. Rosch, *Phys. Rev. Lett.* **109**, 235304 (2012).
- [38] P. R. Johnson, E. Tiesinga, J. V. Porto, and C. J. Williams, *New J. Phys.* **11**, 093022 (2009).
- [39] P. R. Johnson, D. Blume, X. Y. Yin, W. F. Flynn, and E. Tiesinga, *New J. Phys.* **14**, 053037 (2012).
- [40] K. W. Mahmud, L. Jiang, E. Tiesinga, and P. R. Johnson, e-print arXiv:1310.4967 (2013).

## I. SUPPLEMENTARY MATERIAL

We derive analytic results for quench dynamics of a one-dimensional Mott insulator using the strong-coupling expansion [30]. Bosons in an optical lattice are described by the Hubbard Hamiltonian of Eq. 1. We assume a homogeneous system with  $L = 2M + 1$  sites, periodic boundary conditions, and atom number  $N = \bar{n}L$ , where  $M$  and  $\bar{n}$  are positive integers.

We prepare the Mott-insulator ground state assuming a non-zero tunneling energy  $J_i$  that is small compared to the atom-atom interaction strength  $U_i$ . Following [30] we perform perturbation theory in the tunneling operator or kinetic energy. To zeroth-order the ground state wavefunction is the Mott state  $|0\rangle = |\bar{n}, \bar{n}, \dots, \bar{n}\rangle$  with  $\bar{n}$  atoms in each of the  $L$  sites. The correction to this wavefunction is due to states containing a single hole with  $n-1$  atoms in one of the sites and a single ‘‘particle’’ with  $n+1$  atoms in another. We classify these (normalized) particle-hole pair states as

$$|e_d\rangle = \frac{1}{\sqrt{2L}} (\dots + |\dots, \underbrace{\bar{n}-1, \dots, \bar{n}+1}_{d \text{ sites}}, \dots\rangle + \dots \\ \dots + |\dots, \underbrace{\bar{n}+1, \dots, \bar{n}-1}_{d \text{ sites}}, \dots\rangle + \dots),$$

where  $d = 1, \dots, M$  is the number of sites that separates the hole and particle. The dots in a ket indicate sites with  $\bar{n}$  atoms and the sum is over all states with the same particle and hole separation. The hole is either to the left or right of the particle. (Periodic boundary conditions imply that the largest separation is  $M$ .) The Hubbard Hamiltonian within the space spanned by  $\{|0\rangle, |e_1\rangle, \dots, |e_M\rangle\}$  is given by

$$H = \begin{bmatrix} E_0 & A^T \\ A & K \end{bmatrix},$$

where  $E_0 = U_i L \bar{n}(\bar{n}-1)/2$  is the diagonal matrix element for state  $|0\rangle$ ,  $A^T = (-\sqrt{2L\bar{n}(\bar{n}+1)}J_i, 0, 0, 0, \dots)$  with  $M$  elements describes the coupling between  $|e_d\rangle$  and  $|0\rangle$ , and

$$K = \begin{bmatrix} E_0 + U_i & -(2\bar{n}+1)J_i & 0 & \dots \\ -(2\bar{n}+1)J_i & E_0 + U_i & -(2\bar{n}+1)J_i & \dots \\ 0 & -(2\bar{n}+1)J_i & E_0 + U_i & \dots \\ \dots & \dots & \dots & \dots \end{bmatrix}$$

is a  $M \times M$  tridiagonal (diagonal-constant) matrix that describes the couplings among the  $|e_d\rangle$ .

All diagonal elements of  $K$  are the same, and we must first diagonalize  $K$  in order to perform perturbation theory. Its eigenenergies and functions are

$$\mathcal{E}_k = E_0 + U_i - 2(2\bar{n}+1)J_i \cos\left(\frac{\pi k}{M+1}\right)$$

and

$$|\tilde{e}_k\rangle = \sqrt{\frac{2}{M+1}} \sum_{j=1}^M \sin\left(\frac{\pi j k}{M+1}\right) |e_d\rangle.$$

Performing perturbation theory with respect to the non-degenerate states  $|\tilde{e}_k\rangle$ , the correction to the ground state wavefunction is

$$|g\rangle = \left(1 - L\bar{n}(\bar{n}+1)\frac{J_i^2}{U_i^2}\right)|0\rangle + \sqrt{2L\bar{n}(\bar{n}+1)}\frac{J_i}{U_i}|e_1\rangle \\ + (2\bar{n}+1)\sqrt{2L\bar{n}(\bar{n}+1)}\frac{J_i^2}{U_i^2}|e_2\rangle + O[(J_i/U_i)^3]$$

in terms of the original particle-hole basis.

We now quench the system by suddenly setting the tunneling to zero and change  $U_i \rightarrow U_f$ . The subsequent time evolution is then given by

$$|g(t)\rangle = (1 - L\bar{n}(\bar{n}+1)\frac{J_i^2}{U_i^2})|0\rangle \\ + \sqrt{2L\bar{n}(\bar{n}+1)}\frac{J_i}{U_i}|e_1\rangle e^{-iU_f t/\hbar} \\ + (2\bar{n}+1)\sqrt{2L\bar{n}(\bar{n}+1)}\frac{J_i^2}{U_i^2}|e_2\rangle e^{-iU_f t/\hbar} \quad (1)$$

as the states  $|0\rangle$  and  $|e_d\rangle$  are eigenstates of the quenched Hamiltonian. In fact, the  $|e_d\rangle$  are degenerate with an energy  $U_f$  relative to the state  $|0\rangle$ .

Our experimental observables are the quasi-momentum distribution at the  $\Gamma$  point and the edge of the Brillouin zone, defined as  $n_{k=0}(t) = \langle g(t)|b_{k=0}^\dagger b_{k=0}|g(t)\rangle = \sum_{jj'} \rho_{jj'}(t)/L$ , and  $n_{k=\pi}(t) = \sum_{jj'} (-1)^{j-j'} \rho_{jj'}(t)/L$ , respectively. Here  $\rho_{jj'}(t) = \langle g(t)|b_j^\dagger b_{j'}|g(t)\rangle$  is the  $L \times L$  single-particle density matrix. Finally, the visibility is defined by

$$\mathcal{V}(t) = \frac{n_{k=0}(t) - n_{k=\pi}(t)}{n_{k=0}(t) + n_{k=\pi}(t)}.$$

The single-particle density matrix can be evaluated using Eq. 1 and leads to

$$\rho_{jj'}(t) = \left(1 - 2L\bar{n}(\bar{n}+1)\frac{J_i^2}{U_i^2}\right) \langle 0|b_j^\dagger b_{j'}|0\rangle \\ + \sqrt{2L\bar{n}(\bar{n}+1)}\frac{J_i}{U_i} \left(\langle 0|b_j^\dagger b_{j'}|e_1\rangle e^{-iU_f t/\hbar} \right. \\ \left. + \langle e_1|b_j^\dagger b_{j'}|0\rangle e^{iU_f t/\hbar}\right) \\ + (2\bar{n}+1)\sqrt{2L\bar{n}(\bar{n}+1)}\frac{J_i^2}{U_i^2} \\ \times \left(\langle 0|b_j^\dagger b_{j'}|e_2\rangle e^{-iU_f t/\hbar} + \langle e_2|b_j^\dagger b_{j'}|0\rangle e^{iU_f t/\hbar}\right) \\ + 2L\bar{n}(\bar{n}+1)\frac{J_i^2}{U_i^2} \langle e_1|b_j^\dagger b_{j'}|e_1\rangle,$$

to second order in  $J_i/U_i$ . Further analysis shows that  $\rho_{jj'}(t) = \zeta_{|j-j'|}(t)$  is a positive-definite pentadiagonal matrix with diagonal-constant coefficients given by  $\zeta_0(t) = n$ ,  $\zeta_1(t) = 2\bar{n}(\bar{n}+1)(J_i/U_i) \cos(U_f t/\hbar)$ ,  $\zeta_2(t) =$

$\bar{n}(\bar{n}+1)(2\bar{n}+1)(J_i^2/U_i^2)(1+2\cos(U_ft/\hbar))$ , and zero otherwise. In the thermodynamic limit, the quasi-momentum dynamics is given by

$$n_k(t) = \bar{n} + 4\bar{n}(\bar{n}+1)\frac{J_i}{U_i}\cos\left(\frac{U_ft}{\hbar}\right)\cos(k) + 2\bar{n}(\bar{n}+1)(2\bar{n}+1)\frac{J_i^2}{U_i^2}\left[1+2\cos\left(\frac{U_ft}{\hbar}\right)\right]\cos(2k),$$

and the visibility is

$$\mathcal{V}(t) = \frac{4\bar{n}(\bar{n}+1)\frac{J_i}{U_i}\cos(U_ft/\hbar)}{\bar{n}+2\bar{n}(\bar{n}+1)(2\bar{n}+1)\frac{J_i^2}{U_i^2}[1+2\cos U_ft/\hbar]} \approx 4(\bar{n}+1)\frac{J_i}{U_i}\cos(U_ft/\hbar).$$

We find that it is also useful to define  $\lambda_c(t)$ , the largest eigenvalue of the single-particle density matrix at time  $t$ . As  $\rho_{jj'}(t)$  is a real symmetric matrix, we can use perturbation theory to find its largest eigenvalue. We define  $\rho(t) = \rho^{(0)}(t) + \delta\rho(t)$  with tri-diagonal matrix  $\rho^{(0)}(t)$  given by the diagonal and sub- and super-diagonal of  $\rho(t)$ . The matrix  $\rho^{(0)}(t)$  can be diagonalized analytically and its largest eigenvalue is

$$\lambda_c^{(0)}(t) = \bar{n} + 4\bar{n}(\bar{n}+1)\frac{J_i}{U_i}|\cos(U_ft/\hbar)|\cos\left(\frac{\pi}{L+1}\right),$$

with corresponding eigenvector  $\vec{v}$  and elements

$$v_j = \sqrt{\frac{2}{L+1}}\sin\left(\frac{\pi j}{L+1}\right)$$

when  $U_ft/\hbar \in (-\pi/2 + 2\pi m, \pi/2 + 2\pi m)$ , and

$$v_j = \sqrt{\frac{2}{L+1}}(-1)^j\sin\left(\frac{\pi j}{L+1}\right),$$

when  $U_ft/\hbar \in (\pi/2 + 2\pi m, 3\pi/2 + 2\pi m)$ . Here  $m$  is any integer and index  $j = 1, \dots, L$ .

Finally, the matrix  $\delta\rho(t)$  corrects the largest eigenvalue and we have

$$\begin{aligned} \lambda_c(t) &= \lambda_c^{(0)}(t) + \vec{v}^T \cdot \delta\rho(t) \cdot \vec{v} \\ &= \bar{n} + 4\bar{n}(\bar{n}+1)\frac{J_i}{U_i}|\cos(U_ft/\hbar)| \\ &\quad + 2\bar{n}(\bar{n}+1)(2\bar{n}+1)\frac{J_i^2}{U_i^2}[1+2\cos(U_ft/\hbar)], \end{aligned}$$

to first order in  $\delta\rho(t)$ .